THE JOURNAL OF PHYSICAL CHEMISTRY B
A JOURNAL OF THE AMERICAN CHEMICAL SOCIETY

pubs.acs.org/JPCB

Article

# Physical Aging of Poly(methyl methacrylate) Brushes and Spin-Coated Films

*Published as part of The Journal of Physical Chemistry B special issue "Mark Ediger Festschrift".*

Sneha Srinivasan, Allyson L. McGaughey, Zhiyong Jason Ren, Biao Zuo,* and Rodney D. Priestley*

Cite This: *J. Phys. Chem. B* 2024, 128, 11999–12007

Read Online

ACCESS | Metrics & More | Article Recommendations | Supporting Information

**ABSTRACT:** While there is significant attention aimed at understanding how one-dimensional confinement and chain confirmations can impact the glass transition temperature ($T_g$) of polymer films, there remains a limited focus on similar effects on sub-$T_g$ processes, notably, structural relaxation. Using spectroscopic ellipsometry, we investigated the combined influence of confinement and molecular packing on $T_g$ and physical aging, i.e., the property changes that accompany structural relaxation, at select film thicknesses and aging temperatures ($T_a$). We used poly(methyl methacrylate) (PMMA) films in the brush and spin-coated morphologies as model systems. We found that whether a PMMA film exhibited a decrease or increase in physical aging rate with confinement was dependent on the morphology. Notably, PMMA brushes exhibited higher physical aging rates compared to similarly thick spin-coated films at all values of $T_a$. These intriguing findings reveal the strong effects of confinement and molecular packing on the structural relaxation of polymer films. Results from this study have the potential to aid in the design of thin-film materials with controllable long-term glassy-state properties.

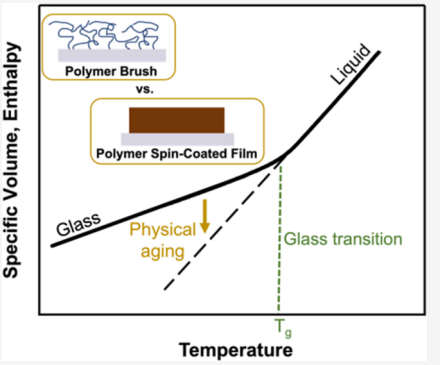




## INTRODUCTION

Below the glass transition temperature ($T_g$), glassy materials will gradually relax via molecular rearrangements toward thermodynamic equilibrium in a process known as structural relaxation.[1−7] The corresponding changes in properties due to structural relaxation are referred to as physical aging, and an understanding of this process is critically important to the design of glassy materials for long-term use applications.[8] Previous studies have reported reduced permeability,[9−12] decreased bending strength,[13] increased elastic modulus,[14] and other temporally dependent material properties due to structural relaxation.[8] With the advancement of nanotechnology, it is imperative to gain a comprehensive understanding of such material properties for glassy polymer films that are one-dimensionally confined. Previous studies have shown that upon confinement, polymer films can exhibit significant changes in physical aging relative to their bulk analogues.[3,7,15,16] Specifically, thin poly(methyl methacrylate) (PMMA)[7] and poly(styrene) (PS)[3] spin-coated films exhibited reduced physical aging rates, and in some instances, ultrathin PS spin-coated films (10 nm) demonstrated a complete absence of physical aging when annealed below bulk $T_g$.[16]

In these physical aging studies,[3,7,16,17] the polymer films were prepared via spin-coating, which enabled control of the final film thickness through a balance of various processing parameters (e.g., solution concentration, rotational speed, etc.).[18] Upon vitrification, the conformation of polymer chains in spin-coated films has been shown to depend on the level of confinement.[19] Additionally, solvent quality[20] and prolonged melt-state annealing[21,22] can promote conformational changes of the polymer chains in spin-coated films. In a previous study, it was shown that extending the melt-state annealing time, and consequently, increasing the thickness of the irreversibly adsorbed layer, reduced $T_g$ deviations in thin spin-coated films of poly(4-*tert*-butylstyrene).[21] This work showed that polymer chain packing plays a significant role in material properties, yet the correlation between physical aging and chain packing in thin films remains unstudied. As such, the following question arises: How do confinement effects and molecular packing combine to influence the physical aging of polymer films?

A polymer brush, which is a film of polymer chains chemisorbed to a substrate through covalent bonding of a single end group,[23] enables simultaneous control of molecular packing and film thickness, representing a unique film morphology that allows us to explore the above critical question. On flat surfaces, which is the surface geometry of interest in this work, the brush morphology is governed by the

**Received:** August 23, 2024
**Revised:** October 29, 2024
**Accepted:** November 1, 2024
**Published:** November 22, 2024

grafting density ($\sigma$, chains/nm$^2$), or the number of polymer chains per unit of the substrate area, and the length, or molecular weight, of the grafted polymers.[24−28] Notably, polymer chain tethering in brushes can often lead to morphologies that are structurally different than spin-coated films.[25−27]

There have been several studies that have focused on $T_g$ measurements of polymer brushes and their key differences compared to spin-coated films.[25−27,29−31] In one study, Zuo et al. systematically demonstrated how the confluence of confinement and morphology impacted the $T_g$ of PS films,[27] reporting a $T_g$ that was 75 °C higher for a 5 nm PS brush in the case of an ultradense grafting density ($\sigma$ = 1.23 chains/nm$^2$) relative to a similarly thick PS spin-coated film.[27] In another example, Yamamoto et al. reported that PMMA brushes ($\sigma \sim$ 0.7 chains/nm$^2$) exhibited $T_g$s at least 8 °C higher than those of PMMA spin-coated films regardless of thickness.[30] In addition to studies on $T_g$, there has been work examining the physical aging of assemblies of polymers grafted onto nanoparticles.[32,33] However, these studies do not isolate the effects of one-dimensional confinement and morphology on physical aging. To our knowledge, there has not been a thorough set of investigations on the physical aging of polymer brushes in the thin-film geometry. Such a study would enable a comparison of the physical aging responses between polymer brushes and spin-coated films.

Here, we employ an approach using ellipsometry developed by Baker et al.,[34] and previously used on diverse film systems,[3,15,35,36] to measure the physical aging of PMMA brushes and spin-coated films. We performed measurements as a function of film thickness ($h$), physical aging temperature ($T_a$), and morphology (i.e., brushes and spin-coated films) to isolate the effects of molecular packing and confinement on the physical aging behavior of PMMA films. Our work shows that film morphology does have a strong influence on structural relaxation of polymer thin films. At quench depths below the $T_g$ of the material, or $T_g(h) - T_a$, the physical aging rate may decrease or increase with confinement depending on the film morphology. PMMA brushes can possess higher physical aging rates compared to similarly thick spin-coated films, with the highest aging rates for PMMA brushes at shallow quench depths that are close to the $T_g$ of the material. Taken together, our study may direct additional routes to tune and predict the long-term behavior of thin films.

## EXPERIMENTAL SECTION

**Materials.** One-sided polished silicon wafers were used as substrates for all experiments (UniversityWafer). Sulfuric acid ($H_2SO_4$, 95.0−98.0%), (3-aminopropyl)triethoxysilane (APTES, > 98.0%), *N,N,N′,N″,N″*-pentamethyldiethylenetriamine (PMDETA, 99%), and methyl methacrylate (MMA, containing ≤30 ppm MEHQ as inhibitor, 99%), and aluminum oxide (activated, basic, Brockman I) were purchased from Sigma-Aldrich. Hydrogen peroxide ($H_2O_2$, 30%, Certified ACS), toluene (HPLC), acetone (Certified ACS), ethanol (200 proof), dichloromethane ($CH_2Cl_2$, HPLC), tetrahydrofuran (THF, HPLC), methanol (HPLC), triethylamine (TEA, ≥99.5%), $\alpha$-bromoisobutyryl bromide (BIBB, 97%), glacial acetic acid (100%), and tetrabutylammonium fluoride (TBAF, 1 M in THF) were purchased from Fisher Scientific. Mirror-finish copper sheets, which were used for PMMA brush polymerization, were purchased from McMaster-Carr. PMMA was purchased from Polymer Source ($M_n$ ranging from 171−450 kg/mol, PDI < 2.1). Prior to use, PMDETA was filtered through a 0.1 $\mu$m polytetrafluoroethylene syringe filter. MMA was passed through an alumina column to remove inhibitors before the monomer was added to the polymerization reaction solution. The materials and protocol to synthesize the fluorescent probe pyrenebutyl methacrylate can be found in a previous report.[22] This fluorescent probe was used in the current study to verify thoroughness of the washing protocol for the PMMA brushes. All other chemicals and materials were used as purchased unless otherwise noted.

**Synthesis and Characterization of Initiator-Immobilized Substrates.** Silica wafers were immersed in a piranha solution (3:1 $H_2SO_4$:$H_2O_2$ v/v) for 2 h at 75 °C. Upon removal, the wafers were sonicated three times in Milli-Q water for 1 min each. Subsequently, the wafers were rinsed with ethanol and dried with a nitrogen stream. The initiator immobilization process was adapted from existing procedures,[25,26] and it is briefly described here. In the first step, the piranha-treated wafers were submerged in a toluene solution with APTES (0.04% v/v) for 24 h at room temperature to produce aminated substrates. Following this reaction, the aminated wafers were sonicated separately in toluene and then acetone for 3 min each. The substrates were again rinsed with ethanol and dried with a nitrogen stream. The dried substrates were placed in a stirred solution of TEA and $CH_2Cl_2$ that was cooled for 10 min using an ice bath. Once cooled, BIBB was injected into the solution, resulting in a final solution of BIBB/TEA/$CH_2Cl_2$ in a ratio of 1:1:20 v/v. After the solution was cooled for another 30 min, the reaction proceeded at room temperature for 15 h while stirring. Subsequently, the BIBB-functionalized substrates were sonicated respectively in $CH_2Cl_2$ and then acetone for 3 min each to remove any unreacted chemical species. Finally, the substrates were rinsed with ethanol and dried with a nitrogen stream.

The successful attachment of the BIBB initiators was confirmed through elemental composition characterization using X-ray photoelectron spectroscopy (XPS, K-Alpha, Thermo Fisher Scientific, Figure S1). Water droplets were deposited on piranha-treated and BIBB-functionalized silica substrates to perform contact angle measurements (Figure S2). Contact angle measurements could not be taken on the hydrophilic piranha-treated silica substrates because the water droplets quickly spread upon contact with the surface. Water contact angle measurements on BIBB-functionalized substrates were performed three times across different locations on the surface.

**Synthesis and Characterization of PMMA Brushes.** PMMA brushes were grafted from BIBB-functionalized wafers using zerovalent copper plate-mediated surface-initiated atom transfer radical polymerization ($Cu^0$-SI-ATRP) through modifications of previously published procedures.[37−43] The polymerization reaction solution consisted of deinhibited MMA (1.54 M) and PMDETA (0.05 M) in water and methanol (2:1 v/v). Before PMMA brush fabrication, the mirror-finish copper plate was washed with 100 mL of acetic acid and then thoroughly dried with a nitrogen stream. The polymerization reaction solution (500 $\mu$L) was pipetted atop the dried copper plate, and the BIBB-functionalized substrate was immediately placed in contact with the reaction solution. A 6 g/cm$^2$ weight was applied to the BIBB-functionalized substrate for all polymerizations. In this setup, the polymerization time indicates the time that the BIBB-functionalized substrate was in contact with the reaction solution, which is


https://doi.org/10.1021/acs.jpcb.4c05704
J. Phys. Chem. B 2024, 128, 11999−12007

used to control the final thickness of the PMMA brush. Notably, this polymerization technique does not require deoxygenation or heat to proceed. At the end of the polymerization, the PMMA brush-modified substrates were sequentially sonicated three times in fresh THF for 20 min each time, or 1 h in total in THF, and afterward, the brushes were sonicated two times in fresh acetone for 15 min each time, or 30 min in total. This sonication procedure was completed to ensure that unreacted monomer species and/or unattached polymer chains were removed.

Thoroughness of the washing protocol was verified through preparation of fluorescently labeled PMMA brushes by adding pyrenebutyl methacrylate (3.05 mM) to the reaction solution prior to brush polymerization. After each washing step of the labeled PMMA brush, the supernatant was collected and excited at $\lambda$ = 340 nm (6 nm slit width) on a spectrofluorometer (Horiba Scientific Fluorolog-QM) to collect the fluorescence spectra. These fluorescence measurements were taken to ensure removal of residual monomeric or polymeric species in the brushes. Following the fourth sonication step, the fluorescence spectra of the supernatant match the spectra of pure acetone (Figure S3), indicating that four washing steps with sonication remove unattached/unwanted species in the PMMA brushes. For thoroughness, the PMMA brushes were subjected to a final wash with pure acetone, totaling to five washing steps with sonication. After sonication, the PMMA brushes were rinsed with ethanol and dried with a nitrogen stream. Finally, the PMMA brushes were placed in an oven heated to 115 °C under vacuum for approximately 12 h. This temperature, which is below $T_{g,bulk}$ of PMMA, was chosen to avoid any unintentional degrafting of the polymer chains from the substrate.[44] Atomic force microscopy (AFM, Bruker NanoMan) was performed on PMMA brush samples at room temperature in tapping mode (Bruker tips, spring constant, $k$ = 40 N/m, resonant frequency, $f_0$ = 300 kHz) to extract information on the homogeneity of the film surface. The AFM scans were analyzed via Gwyddion.

**Chemical Degrafting of PMMA Brushes.** Controlled chemical degrafting was completed by immersing the PMMA brushes in a solution of TBAF (0.04 M) in THF, heated to 50 °C for 10 h, as previously reported in literature.[26,45,46] At the end of the degrafting process, the reaction vessel was sonicated for 10 min, and the reaction solution was pipetted into a round-bottom flask. Subsequently, the substrates were placed in 25 mL of clean THF and further sonicated for 10 min to ensure complete removal of all polymer chains from the substrates. The THF solution was then pipetted into the same round-bottom flask. Finally, the THF in the round-bottom flask was removed using a rotary evaporator until a viscous solution was obtained. $CH_2Cl_2$ and Milli-Q water (1:1 v/v) were added to the viscous solution containing the polymer, and the flask was vigorously shaken to remove aqueous impurities. The organic phase was separated from the aqueous phase three times, using fresh aqueous solution for each separation. After evaporation of the organic phase ($CH_2Cl_2$), up to 1 mL of fresh THF was pipetted onto the degrafted PMMA, and the final solution was shaken. The molecular weight for the polymers was characterized using size exclusion chromatography (SEC).

**Preparation of Spin-Coated PMMA Films.** Prior to spin-coating, silica wafers were immersed in a piranha solution (3:1 $H_2SO_4$:$H_2O_2$ v/v) for 2 h at 75 °C. After piranha treatment, the silica wafers were sonicated three times for 1 min each in Milli-Q water. The wafers were then washed with ethanol and thoroughly dried with a nitrogen stream. Subsequently, PMMA was dissolved in toluene and spin-coated onto piranha-treated silicon wafers. The spin-coated film thickness was controlled by the PMMA concentration in the toluene and the speed of the rotating stage.[18] Upon completion, the PMMA spin-coated films were placed in an oven heated to 115 °C under vacuum for approximately 12 h, similar to the post-synthetic treatment for the PMMA brushes.

**PMMA Film Thickness Characterization.** Thickness measurements for all PMMA films were determined using spectroscopic ellipsometry (M-2000, J.A. Woollam Co.) at an angle of incidence of 70°. The $D_2$ lamp, which controls the UV light source, was turned off for all ellipsometry measurements to avoid potential degradation of PMMA. The collected data were fit to a three-layer model, over a wavelength range of $\lambda$ = 400−1000 nm, consisting of a Cauchy top layer, $n(\lambda) = A + \frac{B}{\lambda^2} + \frac{C}{\lambda^4}$, to determine the dry film thickness, or $h$, of PMMA brushes and spin-coated films. The model has a 2.0 nm native silicon oxide middle layer and a silicon substrate bottom layer.[15,34]

Swollen thickness measurements ($h_{swollen}$) for PMMA brushes were determined via in situ ellipsometry using a 500 $\mu$L horizontal liquid cell (J.A. Woollam Co.) following existing protocols.[47,48] THF was used as the swelling solvent for PMMA brushes. The thickness measurements of each swollen PMMA brush were collected until the rate of thickness change decreased. As described in the literature,[47] the THF optical constants were initially fit with a Cauchy model using a non-swelling calibration wafer of a known thickness, specifically a 25 nm silicon oxide layer on a silicon substrate. The optical constants for THF were unchanged during the thickness fitting of the swollen brushes, where the same three-layer model with a Cauchy top layer was used to fit each swollen PMMA brush thickness. The value of $h_{swollen}$ was taken as the average of measurements in the regime where the rate of thickness change decreased. Swelling ratios ($h_{swollen}/h$) were used to estimate grafting densities ($\sigma$) of PMMA brushes.[47,48]

To study the impact of high temperatures (above bulk $T_g$ of PMMA) on the resulting brush structure, a PMMA brush sample was clamped onto the heat stage (Linkam) attached to the ellipsometer for a specified amount of time at 145 °C. At the end of the desired heat cycle, the PMMA brush was soaked for 10 min in fresh THF, rinsed with acetone and ethanol, and dried with a nitrogen stream. Once dried, the final brush thickness was measured to investigate the extent of degrafting of the PMMA brush from the silica substrate as a result of the heat (Figure S4), which was examined in a previous study for PS brushes.[44] These experiments provided insight into the thermal stability and the extent of polymer chain stretching of the PMMA brushes.

**$T_g$ Measurements.** $T_g$ data of both the PMMA brushes and spin-coated films were obtained via ellipsometry. After annealing above bulk $T_g$ to erase thermal history, $T_g$ measurements were taken at least three times for each sample upon cooling at a rate of 2 °C/min. For each sample of interest, the film thickness data were plotted as a function of temperature to determine $T_g$. In this plot, the glassy and rubbery regimes were each fitted linearly, wherein the $T_g$ was defined as the value corresponding to the intersection of the two lines.[21,49] In this work, $T_g(h)$ represents the $T_g$ of a sample as a function of film thickness, $h$.



https://doi.org/10.1021/acs.jpcb.4c05704
J. Phys. Chem. B 2024, 128, 11999−12007

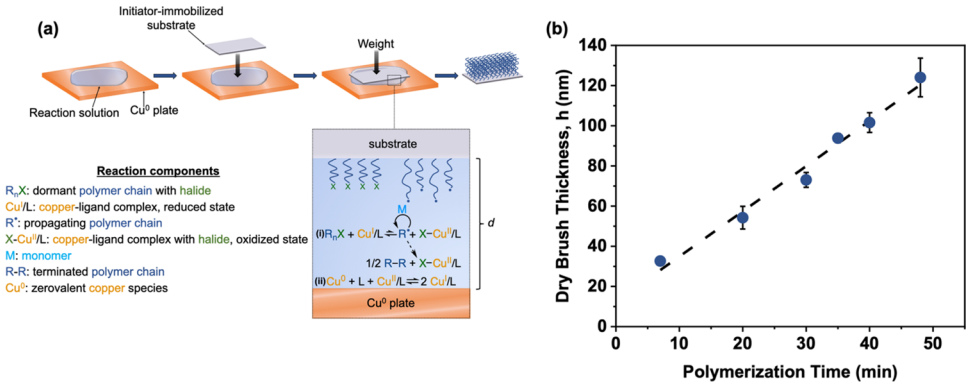


**Figure 1.** (a) $Cu^0$-SI-ATRP experimental setup with the polymerization shown by reaction (i) and the formation of the catalytic species shown by reaction (ii) in the dashed box (legend of reaction components to the left). (b) Dry PMMA brush thickness as a function of polymerization time using $Cu^0$-SI-ATRP. Dashed line indicates linear fit of data from 7 to 48 min. Thickness measurements were taken at least three times at different locations across brush films and averaged. Vertical error bars less than 2 nm were not shown to avoid obscuring data points.

**Physical Aging Measurements.** Physical aging for both PMMA brushes and spin-coated films was investigated via ellipsometry following well-established protocols.[3,15,34] Prior to data collection, the PMMA film was allowed to thermally equilibrate for 10 min at the desired $T_a$ on the Linkam heat stage attached to the ellipsometer, and the sample was then aligned on the ellipsometer at $T_a$. Sample alignment on the ellipsometer was completed before each aging run. After alignment, the films were annealed at a temperature of $T_g(h)$ + 25 °C and then cooled at a rate of 50 °C/min to the selected $T_a$. The cooling rate was kept constant across all aging runs since it is known that the cooling rate impacts the physical aging rate.[50] At $T_a$, thickness measurements were collected for each sample as a function of aging time, with 1 data point collected approximately every 2.4 s for at least 360 min (raw and processed data are shown in Figure S5).

The starting point of the physical aging data analysis was chosen to be at an aging time of 10 min to ensure the sample reached thermal equilibrium at $T_a$. All film thicknesses were normalized by the initial thickness ($h_0$) at this starting point of 10 min, and the subsequent data were averaged over intervals of 10 min. A plot of the normalized film thickness ($h/h_0$) as a function of logarithmic aging time can feature an induction period followed by a steady, linear decrease.[8,15] As described in detail by Baker et al.,[34] the physical aging rate ($\beta$) can be taken as the value of the slope of the data, or $\beta = \frac{-1}{h_0}\frac{dh}{d(\log t)}$, in the linear regime. In our work, we fit the data incrementally to identify the linear region on a logarithmic time scale, starting at an initial point of 10 min until the maximum time of at least 360 min. Subsequently, the data range was contracted toward the linear region by incrementally increasing the value of the initial point of 10 min. The data range that resulted in the linear fit with the maximum $R^2$ value was selected as the best fit for the aging rate calculation. Notably, data ranges with less than 100 data points (i.e., at the tail end of the linear region) were not included to avoid overtrimming the data set and overoptimistic $R^2$ values. All fitting was performed in MATLAB software (version R2020a). The average dry thicknesses of PMMA films selected for physical aging experiments are 31 ± 2 and 110 ± 3 nm for brushes and 30 ± 2 and 111 ± 1 nm for spin-coated films. If rounded to the nearest tenth, the average film thicknesses in this work are between ∼30 and ∼110 nm. Depending on the comparison made in this study, the films are sometimes referred to by this approximation for clarity (e.g., ∼110 nm PMMA brush and spin-coated films refer to two morphologically different films that are similarly thick). At film thicknesses of ∼30 nm in our study, where no induction period was observed, the entire data set starting at 10 min was fit by linear regression on a logarithmic time scale at all $T_a$ for both brush and spin-coated films. To maintain reproducibility, we did not perform physical aging measurements for films less than ∼30 nm due to unreliability in the data at these low thicknesses, which has been previously observed[3] and revealed in our studies as well.

## RESULTS AND DISCUSSION

**Synthetic Control and Characterization of PMMA Brushes.** There have been several modifications of traditional ATRP for growing polymer brushes, which rely on oxygen scavenger mediation by chemical, light, or a metal plate.[42,46,51−54] The experimental setup of $Cu^0$-SI-ATRP, an example of metal plate-mediated ATRP that was used to synthesize PMMA brushes in this work, is shown in Figure 1a, where the polymerization (reaction (i)) proceeds in the liquid layer between the BIBB-functionalized substrate and the $Cu^0$ plate. Previous studies have described a similar experimental setup, in which the distance $d$ between the BIBB-functionalized substrate and the $Cu^0$ plate was estimated to be ∼10 $\mu$m.[37,42] Irreversible termination of the propagating chains can also occur in this reaction. The $Cu^0$ plate acts to rapidly consume the oxygen present, forming a metallic oxide layer where copper species can diffuse.[38,39,41−43,53,55] Reaction (ii) in Figure 1a describes the reaction between the diffused copper species from the metallic oxide layer and the ligand to form activators ($Cu^I$/L) and deactivators ($Cu^{II}$/L) that initiate reaction (i) upon contact with the BIBB-functionalized substrate.

Figure 1b shows a reasonably linear dependency ($R^2$ = 0.982) of the PMMA brush thickness with reaction time. $Cu^0$-SI-ATRP allows access to a range of brush thicknesses that are homogeneous across the film surface (Figure S6), as measured by ellipsometry and AFM. Considering the initial point (0, 0), we note a slightly higher brush growth rate at earlier times (≤7 min) than expected in Figure 1b, similar to trends reported in prior studies that used confined polymerization techniques.[42,56] This subtle change in brush growth rate can potentially be attributed to changes in copper dissolution from the metal plate over time,[57] but a thorough investigation


https://doi.org/10.1021/acs.jpcb.4c05704
J. Phys. Chem. B 2024, 128, 11999−12007

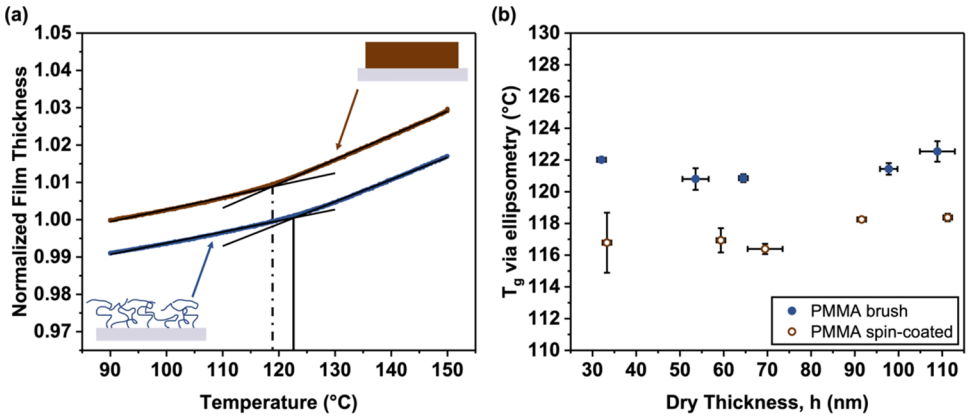


**Figure 2.** (a) Examples of $T_g$ determination by linearly fitting rubbery and glassy regimes for a moderately dense 108 nm PMMA brush (bottom arrow, $T_g$ = 122.9 °C, as indicated by the solid line) and a 113 nm PMMA spin-coated film (upper arrow, $T_g$ = 118.1 °C, as indicated by the dashed line). The thickness is normalized to that at 120 °C for each film morphology, and the data for the PMMA spin-coated film are shifted upward by 0.01 for clarity. (b) PMMA brushes in this study (filled circles) have similar $T_g$ across all $h$. PMMA spin-coated films (unfilled circles) investigated in this work are also shown ($h$ = 33 ± 1 nm, $M_n$ = 171 kg/mol; $h$ = 59 ± 1 nm, $M_n$ = 334 kg/mol; $h$ = 69 ± 4 nm, $M_n$ = 334 kg/mol; $h$ = 92 ± 1 nm, $M_n$ = 450 kg/mol; $h$ = 111 ± 1 nm, $M_n$ = 450 kg/mol).

of the polymerization reaction kinetics is beyond the scope of this work.

Swollen PMMA brush thicknesses were determined via in situ ellipsometry and used to measure the grafting density, or $\sigma$, of the materials, following previously reported protocols using either ellipsometry or AFM.[37,47,48,58] In brief, the equations $\sigma = \frac{\rho * h * N_A}{M_n}$ and $M_n = N * m_0$ describe the relationship between brush parameters, where $\rho$ is the density of bulk polymer (1.18 g/cm$^3$ for PMMA at 20 °C),[28] $h$ is the dry brush thickness, $N_A$ is Avogadro's number, $M_n$ is the number-average molecular weight, $N$ is the degree of polymerization, and $m_0$ is the monomer molecular weight.[47] The value of $N$ depends on $h$ and $h_{swollen}$: $N = \frac{1.074 * h_{swollen}^{3/2}}{h^{1/2}}$.[48] With this approach, it was determined that the PMMA brushes in this study have a $\sigma \sim 0.15$ chains/nm$^2$, which is the average $\sigma$ across three brushes with $h$ = 34, 55, and 105 nm. At this $\sigma$, the PMMA brushes are suggested to be moderately dense.[59] In contrast, PMMA brushes with $\sigma > 0.4$ chains/nm$^2$ are considered to be highly dense,[59] meaning the PMMA brushes in this work are not approaching a highly dense grafting regime. We varied the $M_n$ of the PMMA used to prepare spin-coated films (171−450 kg/mol) to approximately match that of the brush with an equivalent thickness based on these swelling experiments.

SEC was also performed on three different degrafted PMMA brush films with $h$ = 34, 52, 101 nm using TBAF as the chemical agent to cleave the polymer chains from the substrates (Figure S7). There were challenges in degrafting thinner films, specifically at $h$ = 34 and 52 nm, and the SEC curves were quite broad for these brushes. For the thickest PMMA brushes ($h$ = 101 nm) that were degrafted, the sample displayed a sharper SEC curve (Figure S7) with $M_n$ = 310 kg/mol and a polydispersity of 1.95. The $\sigma$ of the PMMA brushes based on the $M_n$ from SEC is ∼0.23 chains/nm$^2$, meaning the brushes can still be classified as moderately dense since $\sigma < 0.4$ chains/nm$^2$.[59] Thermal degrafting of a 68 nm PMMA brush (Figure S4) suggests that the polymer chains are not highly stretched, as there are minimal thickness changes after exposure to a high temperature of 145 °C for 2 h.[44] This finding further supports the calculated $\sigma$ of the PMMA brushes synthesized in this work.

**$T_g$ of PMMA Brushes and Spin-Coated Films.** Figure 2a shows representative ellipsometry data and the approach used to determine $T_g$ for a brush and spin-coated film. For the PMMA brushes investigated in this work, the $T_g$s were 122.0, 120.8, 120.9, 121.4, and 122.5 °C for brush thicknesses of $h$ = 32 ± 1, 54 ± 3, 64 ± 1, 98 ± 2, and 109 ± 4 nm, respectively (Figure 2b). Since the greatest difference in $T_g$ for the PMMA brushes was ∼2 °C, the trend suggests minimal $T_g$ changes across brushes for the thickness range and $\sigma$ used in this study. While $h$ does not influence $T_g$ of PMMA brushes with $\sigma \sim 0.15$ chains/nm$^2$, the $T_g$ of a brush was higher than that of the equivalently thick spin-coated film across all $h$ (Figure 2b). This observation is consistent with earlier investigations[30,60] on PMMA brushes with $0.6 < \sigma < 0.7$ chains/nm$^2$. In a separate report, Zuo et al. demonstrated that a 48 nm PMMA brush ($\sigma$ = 0.77 chains/nm$^2$) had a $T_g$ that was 6 K higher than that of bulk PMMA.[28] This increase in $T_g$ of PMMA brushes upon confinement could be attributed to the higher $\sigma$ of the materials in their work.[28] The higher $T_g$ of PMMA brushes compared to spin-coated films has been suggested to arise from the restricted molecular mobility caused by the covalent attachment of chains to the substrate and extension of polymer chains perpendicular to the surface.[28,30,60]

**Physical Aging Profiles of PMMA Brushes and Spin-Coated Films.** The physical aging curves collected via ellipsometry at $T_a = T_g(h) - 60$ °C are shown in Figure 3 for ∼110 nm thick PMMA brush and spin-coated films. Physical aging curves can be characterized by an induction period at short times, a linear regime at intermediate times, and an equilibrium plateau region at long times on a logarithmic time scale.[8] For both brush and spin-coated films, we observed an induction period for ∼110 nm thick films at specific $T_a$. All PMMA films exhibited a linear regime during aging, where the physical aging rate, or $\beta$, corresponds to the absolute value of the slope in this linear region. Examples of linear fits to determine $\beta$ are also shown in Figure 3 for ∼110 nm thick PMMA brush and spin-coated films. We note that Figures S8 and S9 have additional physical aging curves for ∼110 nm thick PMMA films aged at several different quench depths.



https://doi.org/10.1021/acs.jpcb.4c05704
J. Phys. Chem. B 2024, 128, 11999−12007

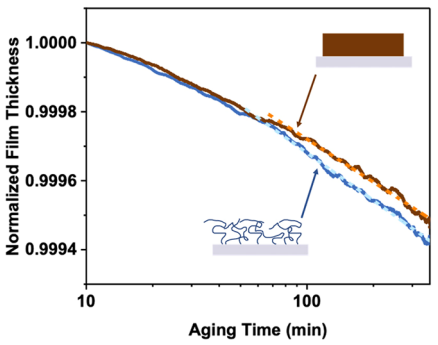


**Figure 3.** Physical aging curves at $T_a = T_g(h) - 60$ °C for a moderately dense PMMA brush (bottom arrow, $\beta = 4.6 \times 10^{-4}$, $h$ = 107 nm) and a PMMA spin-coated film (upper arrow, $\beta = 4.1 \times 10^{-4}$, $h$ = 112 nm). Dashed lines through each data set indicates the linear region determined from the fitting procedure used in this study for ∼110 nm thick PMMA films, where the absolute value of the slope from the fit corresponds to $\beta$.

We performed a similar analysis of the physical aging curves for ∼30 nm thick PMMA brushes and spin-coated films (Figure S10). The physical aging curves did not exhibit an induction period for both ∼30 nm thick brush and spin-coated films. As such, $\beta$ values were determined via fits to the entire physical aging data sets for ∼30 nm thick films. The visible absence of an induction period aligns with previous work by Thees and Roth on PS spin-coated films.[15]

**Comparison of Physical Aging Rates in PMMA Brush and Spin-Coated Films.** The $\beta$ values of ∼30 and ∼110 nm thick PMMA brush and spin-coated films depend on $T_a$ (Figure 4). Irrespective of film morphology and thickness, all

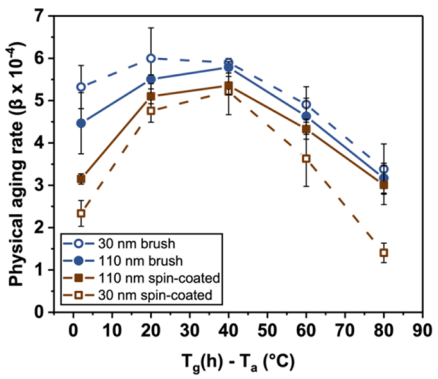


**Figure 4.** Physical aging rates ($\beta$) of the PMMA films investigated in this work as a function of $T_g(h) - T_a$. The line through each data set is provided to enhance visual clarity.

samples displayed a peak in $\beta$ as a function of $T_g(h) - T_a$, i.e., at a specific quench depth below the $T_g$ of the film at thickness, $h$. The peak in $\beta$ is material dependent,[3,7,61] and it is attributed to the interplay between the thermodynamic driving force that enhances physical aging at lower temperatures and molecular mobility that accelerates physical aging at higher temperatures.[3,7,61] The majority of PMMA films in this work exhibit a peak in $\beta$ at a quench depth of approximately $T_g(h) - T_a = 40$ °C. However, for ∼30 nm thick PMMA brushes, there is a slightly shifted peak in $\beta$ closer to the $T_g$ of the material, at approximately $T_g(h) - T_a = 20$ °C. This slight shift suggests that the altered chain packing in the ∼30 nm thick PMMA brushes affects the balance between the thermodynamic driving force toward equilibrium and molecular mobility, ultimately impacting physical aging behavior.[62]

The ∼30 nm thick PMMA brushes have higher $\beta$ values in comparison to those of ∼110 nm thick PMMA brushes at nearly all values of $T_g(h) - T_a$, with the exception of $T_g(h) - T_a = 40$ °C—where the ∼110 nm thick PMMA brushes exhibit a maximum in $\beta$. For spin-coated films, however, film confinement results in a decrease in $\beta$ values across all quench depths, with the largest effects observed away from the peak temperature of $\beta$. These trends demonstrate that the role of confinement on the physical aging response of PMMA depends on film morphology.

Here, the striking difference between brushes and spin-coated films may be attributed to the type of polymer−substrate interactions present in each system. In similar studies on PMMA spin-coated films, Priestley et al. suggested that hydrogen bonding between the ester groups on PMMA and hydroxyl groups on the silica substrate suppresses molecular motion associated with structural relaxation.[7,17] The attractive polymer−substrate interactions in PMMA films supported on silica have also been shown to reduce the dynamics of the material in AFM nanohole relaxation studies.[63] In a separate study, these attractive interactions also suppressed the mobility of thin PS films that were floated on top of the PMMA film.[64] As the thickness of the PMMA spin-coated film is reduced in our work, a larger fraction of the PMMA interacts with the substrate interface relative to the bulk. This fractional increase could result in slower overall physical aging rates due to reduced chain mobility at the interface. At a quench depth of $T_g(h) - T_a = 80$ °C, ∼30 nm thick PMMA spin-coated films exhibit the lowest $\beta$, or $\beta = 1.4 \times 10^{-4}$, across all measurements. The reduced thermal energy at this low temperature could potentially facilitate a greater amount of hydrogen bond formation between the PMMA and silica substrate.

Using similar arguments, PMMA brushes may have a reduced tendency to form hydrogen bonds with the substrate, which could lead to different aging behavior compared to that of the spin-coated analogue. In the brush morphology, each polymer chain has one anchoring point and then extends perpendicularly to the substrate. This extension is particularly notable for brush systems with $\sigma$ values high enough such that the distance between grafted chain ends becomes commensurate to that in size of a degrafted polymer coil, resulting in the chains stretching away from the substrate surface to minimize crowding.[65] Within the proposed experimental system, it is plausible that the extended brush morphology lessens the extent of hydrogen bonding between PMMA and silica compared to spin-coated films due to fewer interaction sites between PMMA side groups and the silica surface. Additionally, it is important to note that the brush synthesis requires substrate modification with BIBB polymerization initiators, which decreases substrate hydrophilicity and overall hydrogen bonding potential (Figure S2). The reduced hydrogen bonding between PMMA and the substrate due to changes in surface chemistry, along with the extended polymer brush structure, supports the experimental observations of enhanced physical aging rates for ∼30 nm thick PMMA brushes.

In addition to thickness comparisons *within* each film morphology, our work enables morphological comparisons *across* films of similar thicknesses. Specifically, ∼ 110 nm thick PMMA brushes exhibit slightly higher $\beta$ across all quench depths in comparison to those of ∼110 nm thick spin-coated


https://doi.org/10.1021/acs.jpcb.4c05704
J. Phys. Chem. B 2024, 128, 11999−12007

films, with the largest difference observed at $T_g(h) - T_a = 2$ °C. When PMMA film thickness is reduced, the difference in $\beta$ is even more pronounced between the brush and spin-coated films. Notably, ∼30 nm thick PMMA brushes age 2.3 and 2.4 times faster than ∼30 nm thick PMMA spin-coated films at $T_g(h) - T_a = 2$ °C and $T_g(h) - T_a = 80$ °C, respectively. These findings highlight the important role of molecular packing on the physical aging response of polymer films in a given state of geometric confinement. Morphological comparisons of similarly thin films serve to further highlight the important role of polymer−substrate interactions within each system.

In addition to the type of interfacial interactions, the resulting structure of PMMA films in the brush morphology could impact the subsequent physical aging response. Previously, it was observed that lower molecular weight PMMA had higher $\beta$ values compared to those of higher molecular weight PMMA at shallow quench depths, or closer to $T_g$ of the material.[62] This trend was correlated to a larger amount of fractional free volume present in the glassy state of the lower molecular weight PMMA.[62] While the $M_n$ between similarly thick PMMA brushes and spin-coated films was kept approximately the same in this work, the polymer chain tethering and chain extension could impact polymer chain conformations and potentially affect the amount of fractional free volume present in PMMA brush systems. Consistent with this argument, we find that ∼30 and ∼110 nm thick PMMA brushes exhibit higher $\beta$ values at shallow quench depths compared to those of their spin-coated counterparts.

Future studies are needed to better understand the mechanistic influence of morphology on the physical aging of polymer films. Previous reports have discussed the impact of structure on the extent of polymer-interface perturbations into the polymer film interior.[25,31,66] Additionally, it has been shown that the brush morphology at high $\sigma$ values can promote local disorder within polymer chains in thin films.[67] There are several inherent differences between PMMA brushes and spin-coated films (i.e., extent of polymer−substrate interactions, chain packing, etc.). While the $T_g$ for both thin-film morphologies do not significantly change with $h$ in this study (Figure 2b), physical aging is impacted to a greater length scale for both brush and spin-coated films, which has been discussed in a prior study for a different system and consistent with our findings.[68]

## CONCLUSIONS

We have investigated the combined influence of confinement and morphology on the physical aging response of PMMA films. Previous studies have focused on the $T_g$s of polymer brush and spin-coated films and separately, the physical aging response of polymer spin-coated films. Our work builds on these studies by investigating both $T_g$ and physical aging, accessed via ellipsometry, on PMMA brushes and spin-coated films at selected thicknesses and quench depths below the $T_g$. We show that within each PMMA film morphology, confinement down to ∼30 nm can lead to different physical aging responses, specifically enhanced or reduced aging rates for brushes and spin-coated films compared to their ∼110 nm analogues, respectively. Across each morphology, the greatest difference in physical aging rates is observed for ∼30 nm PMMA films. Our work provides insight into the potential impact of polymer−substrate interactions and polymer film structure on the physical aging of thin films. Future work will explore the effects of confinement and morphology on the material properties in films of other polymer chemistries.

## ASSOCIATED CONTENT

### Supporting Information

The Supporting Information is available free of charge at https://pubs.acs.org/doi/10.1021/acs.jpcb.4c05704.

XPS characterization and water contact measurements of silica substrates after chemical functionalization, fluorescence spectra of supernatants of dye-labeled PMMA brush after washing steps, PMMA brush thickness measurements after heat exposure, raw physical aging data, surface analysis of PMMA brushes via ellipsometry and AFM, SEC traces, and physical aging curves of PMMA brushes and spin-coated films at several quench depths (PDF)

## AUTHOR INFORMATION


### Corresponding Authors

**Biao Zuo** − *Department of Chemistry, Zhejiang Sci-Tech University, Hangzhou 310018, China;* orcid.org/0000-0002-4921-8823; Email: chemizuo@zstu.edu.cn

**Rodney D. Priestley** − *Department of Chemical and Biological Engineering, Princeton University, Princeton, New Jersey 08544, United States; Princeton Materials Institute, Princeton University, Princeton, New Jersey 08544, United States;* orcid.org/0000-0001-6765-2933; Email: rpriestl@princeton.edu

### Authors

**Sneha Srinivasan** − *Department of Chemical and Biological Engineering, Princeton University, Princeton, New Jersey 08544, United States*

**Allyson L. McGaughey** − *Department of Chemical and Biological Engineering, Princeton University, Princeton, New Jersey 08544, United States; Andlinger Center for Energy and the Environment, Princeton University, Princeton, New Jersey 08544, United States;* orcid.org/0000-0003-0841-3240

**Zhiyong Jason Ren** − *Andlinger Center for Energy and the Environment and Department of Civil and Environmental Engineering, Princeton University, Princeton, New Jersey 08544, United States;* orcid.org/0000-0001-7606-0331

Complete contact information is available at: https://pubs.acs.org/10.1021/acs.jpcb.4c05704


### Notes

The authors declare no competing financial interest.

## ACKNOWLEDGMENTS

The authors acknowledge the use of the Imaging and Analysis Center (IAC) operated by the Princeton Materials Institute at Princeton University, which is supported in part by the Princeton Center for Complex Materials (PCCM), a National Science Foundation (NSF) Materials Research Science and Engineering Center (MRSEC; DMR-2011750). This work was supported by the American Chemical Society (ACS) Petroleum Research Fund (PRF) (62635-ND7). A.L.M. acknowledges funding support from the Andlinger Center for Energy and the Environment, through the Distinguished Postdoctoral Fellowship. B.Z. acknowledges financial support from the National Natural Science Foundation of China (grant numbers. 22122306 and 52373025). The authors thank Prof.

Emily C. Davidson, Shawn M. Maguire, Jason X. Liu, John J. Schreiber, and Denis V. Potapenko for their insightful discussions. The authors also thank Navid Bizmark for guidance on water contact angle measurements.

## REFERENCES

(1) Struik, L. *Physical Aging in Amorphous Polymers and Other Materials*; Elsevier Scientific: Amsterdam, the Netherlands, 1978.
(2) Royal, J. S.; Torkelson, J. M. Monitoring the Molecular Scale Effects of Physical Aging in Polymer Glasses with Fluorescence Probes. *Macromolecules* **1990**, *23* (14), 3536−3538.
(3) Pye, J. E.; Rohald, K. A.; Baker, E. A.; Roth, C. B. Physical Aging in Ultrathin Polystyrene Films: Evidence of a Gradient in Dynamics at the Free Surface and Its Connection to the Glass Transition Temperature Reductions. *Macromolecules* **2010**, *43* (19), 8296−8303.
(4) Zhao, J.; Simon, S. L.; McKenna, G. B. Using 20-Million-Year-Old Amber to Test the Super-Arrhenius Behaviour of Glass-Forming Systems. *Nat. Commun.* **2013**, *4*, No. 1783.
(5) Cangialosi, D.; Boucher, V. M.; Alegría, A.; Colmenero, J. Free Volume Holes Diffusion to Describe Physical Aging in Poly(Mehtyl Methacrylate)/Silica Nanocomposites. *J. Chem. Phys.* **2011**, *135* (1), No. 014901.
(6) Koh, Y. P.; Gao, S.; Simon, S. L. Structural Recovery of a Single Polystyrene Thin Film Using Flash DSC at Low Aging Temperatures. *Polymer* **2016**, *96*, 182−187.
(7) Priestley, R. D.; Ellison, C. J.; Broadbelt, L. J.; Torkelson, J. M. Structural Relaxation of Polymer Glasses at Surfaces, Interfaces, and In Between. *Science* **2005**, *309* (5733), 456−459.
(8) Priestley, R. D. Physical Aging of Confined Glasses. *Soft Matter* **2009**, *5* (5), 919−926.
(9) Huang, Y.; Paul, D. R. Physical Aging of Thin Glassy Polymer Films Monitored by Gas Permeability. *Polymer* **2004**, *45* (25), 8377−8393.
(10) Huang, Y.; Paul, D. R. Effect of Temperature on Physical Aging of Thin Glassy Polymer Films. *Macromolecules* **2005**, *38* (24), 10148−10154.
(11) Huang, Y.; Paul, D. R. Physical Aging of Thin Glassy Polymer Films Monitored by Optical Properties. *Macromolecules* **2006**, *39* (4), 1554−1559.
(12) Huang, Y.; Paul, D. R. Effect of Film Thickness on the Gas-Permeation Characteristics of Glassy Polymer Membranes. *Ind. Eng. Chem. Res.* **2007**, *46* (8), 2342−2347.
(13) Parvatareddy, H.; Wang, J. Z.; Dillard, D. A.; Ward, T. C.; Rogalski, M. E. Environmental Aging of High-Performance Polymeric Composites: Effects on Durability. *Compos. Sci. Technol.* **1995**, *53* (4), 399−409.
(14) Moosburger-Will, J.; Greisel, M.; Horn, S. Physical Aging of Partially Crosslinked RTM6 Epoxy Resin. *J. Appl. Polym. Sci.* **2014**, *131* (23), No. 41121.
(15) Thees, M. F.; Roth, C. B. Unexpected Molecular Weight Dependence to the Physical Aging of Thin Polystyrene Films Present at Ultra-High Molecular Weights. *J. Polym. Sci. B Polym. Phys.* **2019**, *57* (18), 1224−1238.
(16) Kawana, S.; Jones, R. A. L. Effect of Physical Ageing in Thin Glassy Polymer Films. *Eur. Phys. J. E* **2003**, *10* (3), 223−230.
(17) Priestley, R. D.; Broadbelt, L. J.; Torkelson, J. M. Physical Aging of Ultrathin Polymer Films Above and Below the Bulk Glass Transition Temperature: Effects of Attractive vs Neutral Polymer-Substrate Interactions Measured by Fluorescence. *Macromolecules* **2005**, *38* (3), 654−657.
(18) Hall, D. B.; Underhill, P.; Torkelson, J. M. Spin Coating of Thin and Ultrathin Polymer Films. *Polym. Eng. Sci.* **1998**, *38* (12), 2039−2045.
(19) Pressly, J. F.; Riggleman, R. A.; Winey, K. I. Increased Polymer Diffusivity in Thin-Film Confinement. *Macromolecules* **2019**, *52* (16), 6116−6125.
(20) Li, R. N.; Clough, A.; Yang, Z.; Tsui, O. K. C. Equilibration of Polymer Films Cast from Solutions with Different Solvent Qualities. *Macromolecules* **2012**, *45* (2), 1085−1089.
(21) Perez-De-Eulate, N. G.; Sferrazza, M.; Cangialosi, D.; Napolitano, S. Irreversible Adsorption Erases the Free Surface Effect on the $T_g$ of Supported Films of Poly(4-Tert-Butylstyrene). *ACS Macro Lett.* **2017**, *6* (4), 354−358.
(22) Burroughs, M. J.; Napolitano, S.; Cangialosi, D.; Priestley, R. D. Direct Measurement of Glass Transition Temperature in Exposed and Buried Adsorbed Polymer Nanolayers. *Macromolecules* **2016**, *49* (12), 4647−4655.
(23) Milner, S. T. Polymer Brushes. *Science* **1991**, *251* (4996), 905−914.
(24) Zhao, B.; Brittain, W. J. Polymer Brushes: Surface-Immobilized Macromolecules. *Prog. Polym. Sci.* **2000**, *25* (5), 677−710.
(25) Lan, T.; Torkelson, J. M. Substantial Spatial Heterogeneity and Tunability of Glass Transition Temperature Observed with Dense Polymer Brushes Prepared by ARGET ATRP. *Polymer* **2015**, *64*, 183−192.
(26) Zuo, B.; Zhang, S.; Niu, C.; Zhou, H.; Sun, S.; Wang, X. Grafting Density Dominant Glass Transition of Dry Polystyrene Brushes. *Soft Matter* **2017**, *13* (13), 2426−2436.
(27) Zuo, B.; Li, C.; Xu, Q.; Randazzo, K.; Jiang, N.; Wang, X.; Priestley, R. D. Ultrastable Glassy Polymer Films with an Ultradense Brush Morphology. *ACS Nano* **2021**, *15* (6), 9568−9576.
(28) Zuo, B.; Xu, Q.; Jin, T.; Xing, H.; Shi, J.; Hao, Z.; Zhang, L.; Tanaka, K.; Wang, X. Suppressed Surface Reorganization in a High-Density Poly(Methyl Methacrylate) Brush. *Langmuir* **2019**, *35* (46), 14890−14895.
(29) Keddie, J. L.; Jones, R. A. L. Glass Transition Behavior in Ultra-Thin Polystyrene Films. *Isr. J. Chem.* **1995**, *35* (1), 21−26.
(30) Yamamoto, S.; Tsujii, Y.; Fukuda, T. Glass Transition Temperatures of High-Density Poly(Methyl Methacrylate) Brushes. *Macromolecules* **2002**, *35* (16), 6077−6079.
(31) Lan, T.; Torkelson, J. M. Fragility-Confinement Effects: Apparent Universality as a Function of Scaled Thickness in Films of Freely Deposited, Linear Polymer and Its Absence in Densely Grafted Brushes. *Macromolecules* **2016**, *49* (4), 1331−1343.
(32) Koerner, H.; Opsitnick, E.; Grabowski, C. A.; Drummy, L. F.; Hsiao, M. S.; Che, J.; Pike, M.; Person, V.; Bockstaller, M. R.; Meth, J. S.; Vaia, R. A. Physical Aging and Glass Transition of Hairy Nanoparticle Assemblies. *J. Polym. Sci., Part B: Polym. Phys.* **2016**, *54* (2), 319−330.
(33) Bilchak, C. R.; Buenning, E.; Asai, M.; Zhang, K.; Durning, C. J.; Kumar, S. K.; Huang, Y.; Benicewicz, B. C.; Gidley, D. W.; Cheng, S.; et al. Polymer-Grafted Nanoparticle Membranes with Controllable Free Volume. *Macromolecules* **2017**, *50* (18), 7111−7120.
(34) Baker, E. A.; Rittigstein, P.; Torkelson, J. M.; Roth, C. B. Streamlined Ellipsometry Procedure for Characterizing Physical Aging Rates of Thin Polymer Films. *J. Polym. Sci., Part B: Polym. Phys.* **2009**, *47* (24), 2509−2519.
(35) Jin, K.; Li, L.; Torkelson, J. M. Bulk Physical Aging Behavior of Cross-Linked Polystyrene Compared to Its Linear Precursor: Effects of Cross-Linking and Aging Temperature. *Polymer* **2017**, *115*, 197−203.
(36) Frieberg, B. R.; Glynos, E.; Sakellariou, G.; Tyagi, M.; Green, P. F. Effect of Molecular Stiffness on the Physical Aging of Polymers. *Macromolecules* **2020**, *53* (18), 7684−7690.
(37) Yan, W.; Fantin, M.; Ramakrishna, S.; Spencer, N. D.; Matyjaszewski, K.; Benetti, E. M. Growing Polymer Brushes from a Variety of Substrates under Ambient Conditions by $Cu^0$-Mediated Surface-Initiated ATRP. *ACS Appl. Mater. Interfaces* **2019**, *11* (30), 27470−27477.
(38) Li, W.; Sheng, W.; Li, B.; Jordan, R. Surface Grafting "Band-Aid" for "Everyone": Filter Paper-Assisted Surface-Initiated Polymerization in the Presence of Air. *Angew. Chem., Int. Ed.* **2021**, *60* (24), 13621−13625.
(39) Zhang, T.; Du, Y.; Kalbacova, J.; Schubel, R.; Rodriguez, R. D.; Chen, T.; Zahn, D. R. T.; Jordan, R. Wafer-Scale Synthesis of Defined


https://doi.org/10.1021/acs.jpcb.4c05704
J. Phys. Chem. B 2024, 128, 11999−12007

Polymer Brushes under Ambient Conditions. *Polym. Chem.* **2015**, *6* (47), 8176−8183.
(40) Zhang, T.; Du, Y.; Müller, F.; Amin, I.; Jordan, R. Surface-Initiated Cu(0) Mediated Controlled Radical Polymerization (SI-CuCRP) Using a Copper Plate. *Polym. Chem.* **2015**, *6* (14), 2726−2733.
(41) Li, W.; Sheng, W.; Jordan, R.; Zhang, T. Boosting or Moderating Surface-Initiated Cu(0)-Mediated Controlled Radical Polymerization with External Additives. *Polym. Chem.* **2020**, *11* (43), 6971−6977.
(42) Yan, W.; Fantin, M.; Spencer, N. D.; Matyjaszewski, K.; Benetti, E. M. Translating Surface-Initiated Atom Transfer Radical Polymerization into Technology: The Mechanism of $Cu^0$-Mediated SI-ATRP under Environmental Conditions. *ACS Macro Lett.* **2019**, *8* (7), 865−870.
(43) Che, Y.; Zhang, T.; Du, Y.; Amin, I.; Marschelke, C.; Jordan, R. On Water" Surface-Initiated Polymerization of Hydrophobic Monomers. *Angew. Chem., Int. Ed.* **2018**, *57* (50), 16380−16384.
(44) Wang, F.; Liu, W.; Lu, R.; Huang, J. H.; Zuo, B.; Wang, X. Entropy-Enhanced Mechanochemical Activation for Thermal Degrafting of Surface-Tethered Dry Polystyrene Brushes. *ACS Macro Lett.* **2022**, *11* (8), 1041−1048.
(45) Patil, R. R.; Turgman-Cohen, S.; Šrogl, J.; Kiserow, D.; Genzer, J. Direct Measurement of Molecular Weight and Grafting Density by Controlled and Quantitative Degrafting of Surface-Anchored Poly(Methyl Methacrylate). *ACS Macro Lett.* **2015**, *4* (2), 251−254.
(46) Yan, W.; Dadashi-Silab, S.; Matyjaszewski, K.; Spencer, N. D.; Benetti, E. M. Surface-Initiated Photoinduced ATRP: Mechanism, Oxygen Tolerance, and Temporal Control during the Synthesis of Polymer Brushes. *Macromolecules* **2020**, *53* (8), 2801−2810.
(47) Li, M.; Fromel, M.; Ranaweera, D.; Pester, C. W. Comparison of Long-Term Stability of Initiating Monolayers in Surface-Initiated Controlled Radical Polymerizations. *Macromol. Rapid Commun.* **2020**, *41* (17), No. 2000337.
(48) Narupai, B.; Page, Z. A.; Treat, N. J.; McGrath, A. J.; Pester, C. W.; Discekici, E. H.; Dolinski, N. D.; Meyers, G. F.; Read de Alaniz, J.; Hawker, C. J. Simultaneous Preparation of Multiple Polymer Brushes under Ambient Conditions Using Microliter Volumes. *Angew. Chem., Int. Ed.* **2018**, *57* (41), 13433−13438.
(49) Merrill, J. H.; Li, R.; Roth, C. B. End-Tethered Chains Increase the Local Glass Transition Temperature of Matrix Chains by 45 K Next to Solid Substrates Independent of Chain Length. *ACS Macro Lett.* **2023**, *12* (1), 1−7.
(50) Gray, L. A. G.; Yoon, S. W.; Pahner, W. A.; Davidheiser, J. E.; Roth, C. B. Importance of Quench Conditions on the Subsequent Physical Aging Rate of Glassy Polymer Films. *Macromolecules* **2012**, *45* (3), 1701−1709.
(51) Discekici, E. H.; Pester, C. W.; Treat, N. J.; Lawrence, J.; Mattson, K. M.; Narupai, B.; Toumayan, E. P.; Luo, Y.; McGrath, A. J.; Clark, P. G.; et al. Simple Benchtop Approach to Polymer Brush Nanostructures Using Visible-Light-Mediated Metal-Free Atom Transfer Radical Polymerization. *ACS Macro Lett.* **2016**, *5* (2), 258−262.
(52) Zhang, K.; Yan, W.; Simic, R.; Benetti, E. M.; Spencer, N. D. Versatile Surface Modification of Hydrogels by Surface-Initiated, $Cu^0$-Mediated Controlled Radical Polymerization. *ACS Appl. Mater. Interfaces* **2020**, *12* (5), 6761−6767.
(53) Albers, R. F.; Magrini, T.; Romio, M.; Leite, E. R.; Libanori, R.; Studart, A. R.; Benetti, E. M. Fabrication of Three-Dimensional Polymer-Brush Gradients within Elastomeric Supports by $Cu^0$-Mediated Surface-Initiated ATRP. *ACS Macro Lett.* **2021**, *10* (9), 1099−1106.
(54) Matyjaszewski, K.; Hongchen, D.; Jakubowski, W.; Pietrasik, J.; Kusumo, A. Grafting from Surfaces for "Everyone": ARGET ATRP in the Presence of Air. *Langmuir* **2007**, *23* (8), 4528−4531.
(55) McGaughey, A. L.; Srinivasan, S.; Zhao, T.; Christie, K. S. S.; Ren, Z. J.; Priestley, R. D. Scalable Zwitterionic Polymer Brushes for Antifouling Membranes via Cu0-Mediated Atom Transfer Radical Polymerization. *ACS Appl. Polym. Mater.* **2023**, *5* (7), 4921−4932.
(56) Benetti, E. M.; Kang, C.; Mandal, J.; Divandari, M.; Spencer, N. D. Modulation of Surface-Initiated ATRP by Confinement: Mechanism and Applications. *Macromolecules* **2017**, *50* (15), 5711−5718.
(57) Fantin, M.; Ramakrishna, S. N.; Yan, J.; Yan, W.; Divandari, M.; Spencer, N. D.; Matyjaszewski, K.; Benetti, E. M. The Role of $Cu^0$ in Surface-Initiated Atom Transfer Radical Polymerization: Tuning Catalyst Dissolution for Tailoring Polymer Interfaces. *Macromolecules* **2018**, *51* (17), 6825−6835.
(58) Harris, B. P.; Metters, A. T. Generation and Characterization of Photopolymerized Polymer Brush Gradients. *Macromolecules* **2006**, *39* (8), 2764−2772.
(59) Moh, L. C. H.; Losego, M. D.; Braun, P. V. Solvent Quality Effects on Scaling Behavior of Poly(Methyl Methacrylate) Brushes in the Moderate- and High-Density Regimes. *Langmuir* **2011**, *27* (7), 3698−3702.
(60) Erber, M.; Tress, M.; Mapesa, E. U.; Serghei, A.; Eichhorn, K. J.; Voit, B.; Kremer, F. Glassy Dynamics and Glass Transition in Thin Polymer Layers of PMMA Deposited on Different Substrates. *Macromolecules* **2010**, *43* (18), 7729−7733.
(61) Greiner, R.; Schwarzl, F. R. Thermal Contraction and Volume Relaxation of Amorphous Polymers. *Rheol. Acta* **1984**, *23* (4), 378−395.
(62) Wang, T.; Wei, T.; Lin, X.; Torkelson, J. M. Tunability and Molecular Weight Dependence of the Physical Aging Behavior of Polystyrene and Poly(Methyl Methacrylate) Films. *Polym. Eng. Sci.* **2024**, *64* (8), 3869−3883.
(63) Qi, D.; Fakhraai, Z.; Forrest, J. A. Substrate and Chain Size Dependence of near Surface Dynamics of Glassy Polymers. *Phys. Rev. Lett.* **2008**, *101* (9), No. 096101.
(64) Roth, C. B.; McNerny, K. L.; Jager, W. F.; Torkelson, J. M. Eliminating the Enhanced Mobility at the Free Surface of Polystyrene: Fluorescence Studies of the Glass Transition Temperature in Thin Bilayer Films of Immiscible Polymers. *Macromolecules* **2007**, *40* (7), 2568−2574.
(65) Green, P. F. The Structure of Chain End-Grafted Nanoparticle/Homopolymer Nanocomposites. *Soft Matter* **2011**, *7* (18), 7914−7926.
(66) Zhang, C.; Li, L.; Chen, J.; Yang, Y.; Zuo, B.; Li, J.; Wang, X. Chemical Structure Dependence of Surface Layer Thickness on Polymer Films. *J. Phys. Chem. C* **2020**, *124* (23), 12448−12456.
(67) Jin, T.; Zha, H.; Randazzo, K.; Zuo, B.; Priestley, R. D.; Wang, X. Local Disorder Facilitates Chain Stretching in Crowded Polymer Brushes. *J. Phys. Chem. Lett.* **2020**, *11* (18), 7814−7818.
(68) Boucher, V. M.; Cangialosi, D.; Alegría, A.; Colmenero, J. Enthalpy Recovery in Nanometer to Micrometer Thick Polystyrene Films. *Macromolecules* **2012**, *45* (12), 5296−5306.


https://doi.org/10.1021/acs.jpcb.4c05704
*J. Phys. Chem. B* 2024, 128, 11999−12007